Single-step wet-process formation of dual-layer superslippery coating with transparency and robust omniphobicity

Mizuki Tenjimbayashi, Gen Hayase, Takashi Hiroi, Takeshi Ueki*
M. T. Author 1, G. H. Author 2
International Center for Materials Nanoarchitectonics (MANA), National Institute for Materials Science (NIMS), Tsukuba, Ibaraki 305-0044, Japan
E-mail: TENJIMBAYASHI.Mizuki@nims.go.jp
T. H. Author 3
International Center for Young Scientists (ICYS), National Institute for Materials Science (NIMS), Tsukuba, Ibaraki 305-0047, Japan
T. U. Author 4
Research Center for Functional Materials, National Institute for Materials Science (NIMS), Tsukuba, Ibaraki 305-0044, Japan; Graduate School of Life Science, Hokkaido University, Kita 10, Nishi 8, Kita-ku, Sapporo 060-0810, Japan

Keywords: Omniphobicity, superslippery surface, single step wet process, phase separation, clogging transition

Robust coatings that fully repel liquids have a broad range of applications. However, it remains challenging to have an easy, scalable, and substrate-independent preparation method for these coatings. In this study, a coating solution that forms stable lubricant surface-to-solid substrates simply by casting, dipping, or spraying without specific limitation in the substrate character, was synthesized. Furthermore, the thermodynamic stability of the coating and the requirement for the components of coating solution were studied. The coating was transparent (>90%), self-healable, mechanically robust, and repels immiscible liquid droplets, including water, oil, solvent, and fluorinated polymers, with extremely low sliding angle. The functional coating comprised two layers: a lubricant stabilizing base layer (BL) and a top lubricant layer (LL). Generally, two-step coating processes require two layers; however, the coating solution forms the coating only by casting, dipping, or spraying without substrate limitation. Moreover, the coating is formed inside the long narrow tube by flowing the solution. The solution constitutes nanoparticles, a silicone binder, and a binary mixture of a lubricant and a suitable solvent. Lubricant droplets were formed at the air–solution interface to cast the solution on a solid substrate; the droplets coalesced into a LL on top of the coating solution,

and the nanoparticles aggregated at the substrate–solution interface and fixed by the binder to form a BL below the LL. This extremely simple and universal coating approach for robust omniphobic surface preparation is widely applicable for various applications.

1. Introduction

The rapid and complete removal of liquids from surfaces is essential for applications such as anti-fouling, anti-icing, and anti-bacterial coatings, water harvesting, and droplet manipulation. [1–3] To repel liquids with low sliding angles, superhydrophobic [4–6] and superomniphobic surfaces [7–9] have been proposed. Such surfaces are achieved by a controlled nano- to micrometer scale surface texture with low surface energy. In particular, to achieve superomniphobicity, re-entrant structures with surface fluorination or doubly re-entrant structures are required. [7–9] On these surfaces, the droplet−surface contact area is minimized by introducing an air layer between the droplet and the fine textured surfaces, causing the liquid droplet to roll off the surfaces. [10] This so-called Cassie-state is metastable and can collapse under external pressure. Moreover, these surfaces are typically opaque and fragile due to the surface rough structure. [9, 11] Notwithstanding the development of functional superhydrophobic/superomniphobic surfaces, the design of these surfaces still requires highly controlled methods, [12] and there is still a limitation in the repellence of low surface energy liquids (e.g., solvents and fluorine agents), mechanical durability, and stability under pressure. [13]

Another type of liquid repellent surface, liquid-infused surfaces (LIS) [13–15] repel liquids by introducing a stable lubricant layer on the solid surface. On LIS, immiscible liquid droplet slides off because of the lubricity of the surface. An LIS comprises two layers: (i) lubricant stabilizing base layer (BL) and (ii) lubricant layer (LL) on top of it. The BL is a nano -to-micrometer porous solid with a high affinity to the lubricant designed by self-assembling nanomaterials, phase separations, templating, crystal growth, and etching processes.[16] The LL comprises a nonvolatile inert liquid such as silicone oil, fluorinated polymer, fatty acid, or liquid paraffin,[17] and it is formed by simply casting, spreading the lubricant on the BL, and removing the excess by shearing the lubricant or tilting the BL. Further, through appropriate material selection, it is possible to realize optical transparency and a self-repairing function. [13,14]

Overall, LIS is promising for achieving a robust omniphobic surface. In particular, the facile preparation of the LIS while maintaining the LIS function is promising. Efforts have been made to towards the facile preparation of LIS for practical use. [18, 19] However, two-step coating processes are required in most cases to form LIS as it comprises two layers of BL and LL. The two-step coating method requires more processing time and cost compared to a single step coating, and these requirements can become significant when considering large-scale production. Few works succeeded to form organogel-type LIS by one-step curing of the

lubricant−gel precursor mixture, [20-22] which are promising for the moldable self-standing LIS. In other approaches, ideas to covalently attach LL on the solid substrates have been proposed; [23–25] however, the attachment deteriorates the surface lubricity, and the coating substrate is limited to reactive ones. [23] Therefore, an easy and substrate-independent preparation method for robust omniphobic surface preparation is required.

To this end, a coating solution that forms the LIS only by casting, dipping, or spraying it onto a solid substrate was designed. When casting the solution on to a solid substrate, lubricant droplets are formed at the air–solution interface, which coalesce to become the LL on the top of the coating solution whereas the nanoparticles and binder form a hydrophobic porous network at the substrate–solution interface. The coated surface exhibits transparency and robust self-repairing omniphobicity. Further, the coating is transparent and can be formed on the various solid substrate independent of the substrate surface energy via various wet processes. In this study, the mechanism, and requirements for the coating solution to form a thermodynamically stable lubricant coating are investigated. Further, a spray-coated car-window surface was shown to fully repel water shower without external assistance (i.e., inertia and air resisting forces by car acceleration).

2. Results & Discussion

2.1. Concept and Applicability

The concept of this study is developing a coating solution that forms LIS by simply casting it on a solid substrate (**Figure 1**A). This one-step LIS formation is demonstrated in Movie S1. The coating solution comprises nanoparticles (10–100 nm sized fumed/colloidal metal oxide hydrophobic/hydrophilic nanoparticles can be used, Table S1, Figure S1-S4), hydrophobic/lubricant-philic binder room-temperature vulcanizing silicone (RTV silicone, either the one-pack or two-pack type can be used, Table S2), and a mixture of a lubricant and a suitable solvent (Figure S5, S6 for lubricant and solvent selection). This study used the mixture of hydrophobic fumed silica nanoparticles, one-pack type RTV silicone, silicone oil, and isopropanol. The lubricant fraction in the coating solution, Φ_{lub} (lubricant volume per total coating solution volume) is 0.28; the mixture is homogeneous (Figure 1B) and stable at least for 3 months as the solvent protects the RTV silicone from moisture. The liquid repellency of the coated surface was insignificant when the mixture contents were modified (Figure S7). The cast solution is initially homogeneous, but it forms a BL and an LL with time when the mixture is cast on a glass substrate. The focus stack bright field image of the coated surface indicates that a porous network structure is formed below the LL (Figure 1C). The coating is transparent and can be formed on various solid substrates with a wet process including casting, dipping, spraying, and flowing (Movie S2). Examples include a spray-coated surface on glass and stainless steel (Figure 2A), dip-coated surface on aluminum, polycarbonate, nitrile rubber plates (Figure 2B), and the inner layer of silicone rubber tubes formed simply by flowing the coating solution through the tubes (Figure 2C-E). Notably, forming the liquid-repellent coating inside a narrow long tube has been required multi-steps.[26] Figure 2D shows that 200 μL water droplets pass through the silicone tube ~50 times faster with the coating inside the silicone tube with a 30° tilting.

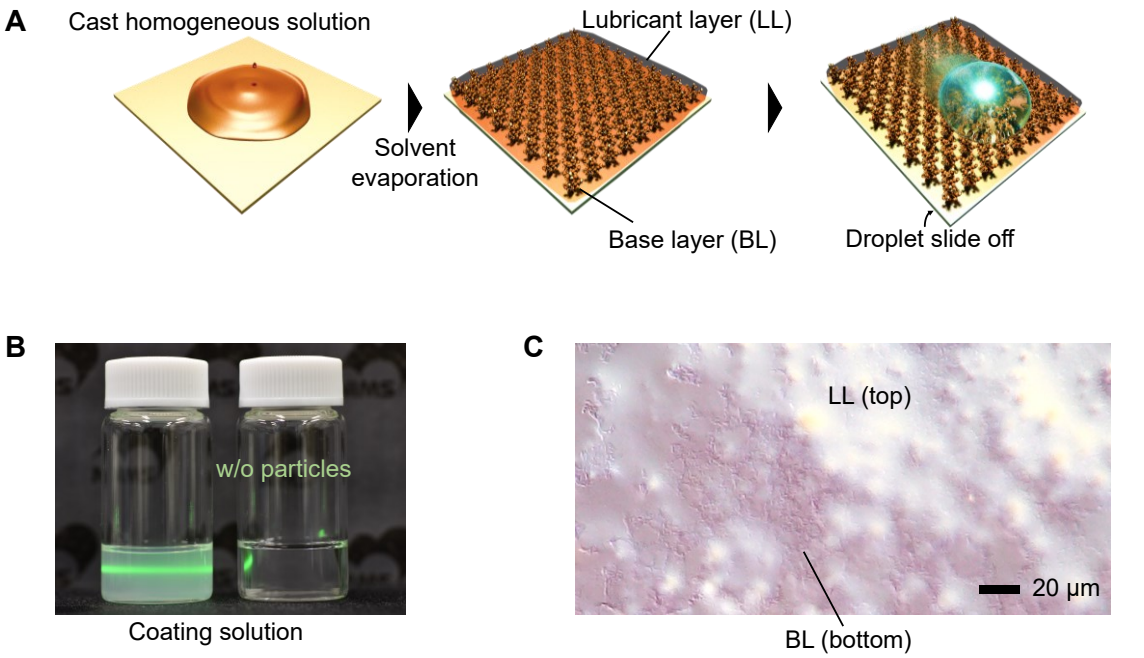

Figure 1. (A) Schematic of the LIS formation process. (B) Photographic image of the coating solution bottle (left) and that without the dispersing particles (right) irradiated by a laser pointer. The lubricant, solvent, and resin mixture is a homogeneous solution, which is confirmed by the absence of Tyndall scattering. (C) Top view focus stack bright field microscopic image of the LIS formed by casting the coating solution.

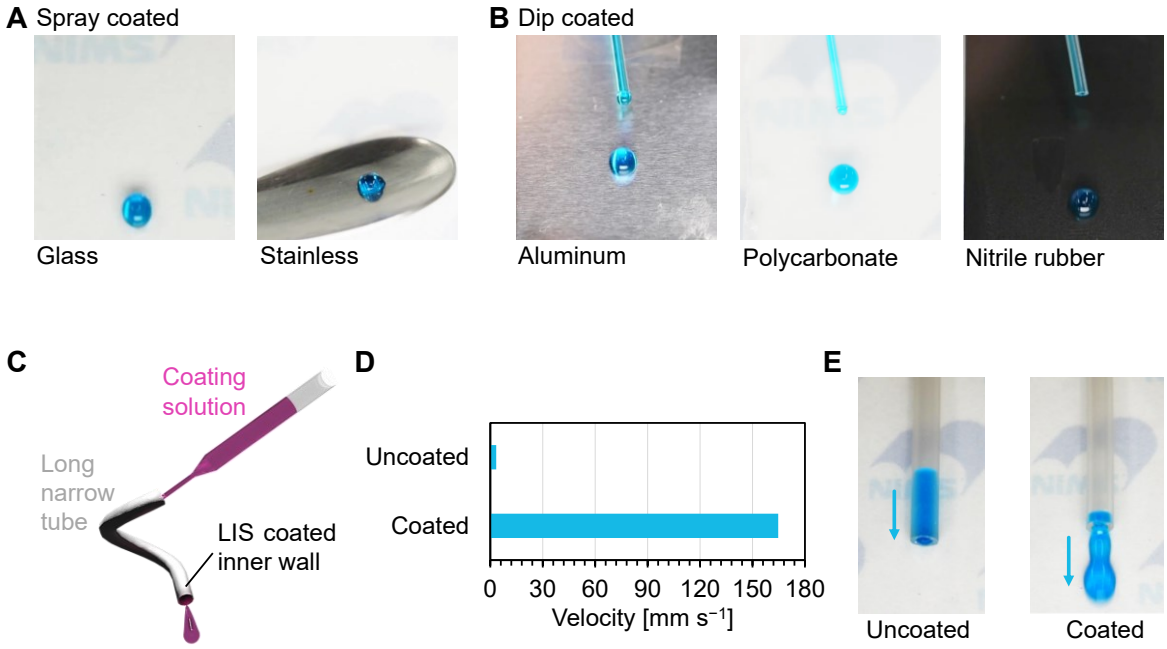

Figure 2. (A, B) Photographs of water droplets on (A) the LIS-spray-coated glass plate and stainless spatula, (B) LIS-dip-coated aluminum, polycarbonate, and nitrile rubber plates. (C)

A schematic of LIS-coated silicone tube by flowing the coating solution on inner the wall. (D) A 200-μL water droplet transportation velocity inside the silicone tube tilted at 30° through the LIS coating. (E) Photographs of water droplets transportation inside the silicone tube.

2.2. Mechanism of Stable Lubricant Surface Formation

A schematic of the LIS formation mechanism is presented in **Figure 3**A. The solvent starts evaporating at the solution−air interface when the homogeneous coating solution is cast on the glass substrate. Through solvent evaporation, lubricant droplets are nucleated, which coalesce with each other to grow in size and form the LL from the edge to the center of the droplet, as shown in Figure 3B. The phases of the lubricant or the solvent are confirmed by observing the dynamic behavior of the lubricant/dyed-solvent mixture droplet (Figure S8). This lubrication system has some dynamic analogy to the Ouzo lubrication system: [27,28] the oil micro droplet is nucleated from the water/oil/ethanol mixture via the evaporation of ethanol. However, the water content in the solvent is 0.24 ± 0.0016% in this work, which is insufficient to induce the Ouzo effect. [29] The shape becomes similar to how the lubricant film cloaks the solvent droplet because of the phase separation between the solvent and the LL; this is confirmed by the existence of a wetting ridge of the lubricant at the droplet edge. [30] The growth of the droplet edge of the lubricants is observed using reflection interference contrast microscopy (RICM) (Figure S9). The edge growth is visualized by the temporal variation of the interference pattern. A typical interference pattern is shown in Figure 3C. The shape of the edge is confirmed to be the wetting ridge, which indicates the phase separation between the solvent and the LL. [27, 30] The LL and BL formation dynamics are monitored through differential interference contrast (DIC) and dark field (DF) microscopic observations, respectively. The DIC observation, which visualizes the difference of the refractive index of silicone oil and the solution, clarifies the time-lapsed images of the surface LL formation from droplet edge to the center (Figure 3D, Movie S3). Meanwhile, the BL formation behavior is visualized by DF observation, which detects only the scattered and reflected light, as shown in Figure 3E (and Movie S3). From the capillary flow, particles are initially transported to the droplet edge. At this stage, the particles are mobile because they are not clogged. The packing density of the particles is increased and they get clogged because of the increase in the number of transported particles. Finally, the particles are fixed by the hydrophobic resin, and the BL is formed below the LL. A nanostructured solid with chemical affinity to LL is promising for BL. [22] Here, the particles' surface is covered with the hydrophobic resin with chemical affinity to LL; thus, the nanoparticles' wide size range and wettability are available for the coating solution (Table S1). Moreover, the coating adheres to the substrate with van der Waals interaction. Therefore, the coating can be formed on various substrates (Figure 2).

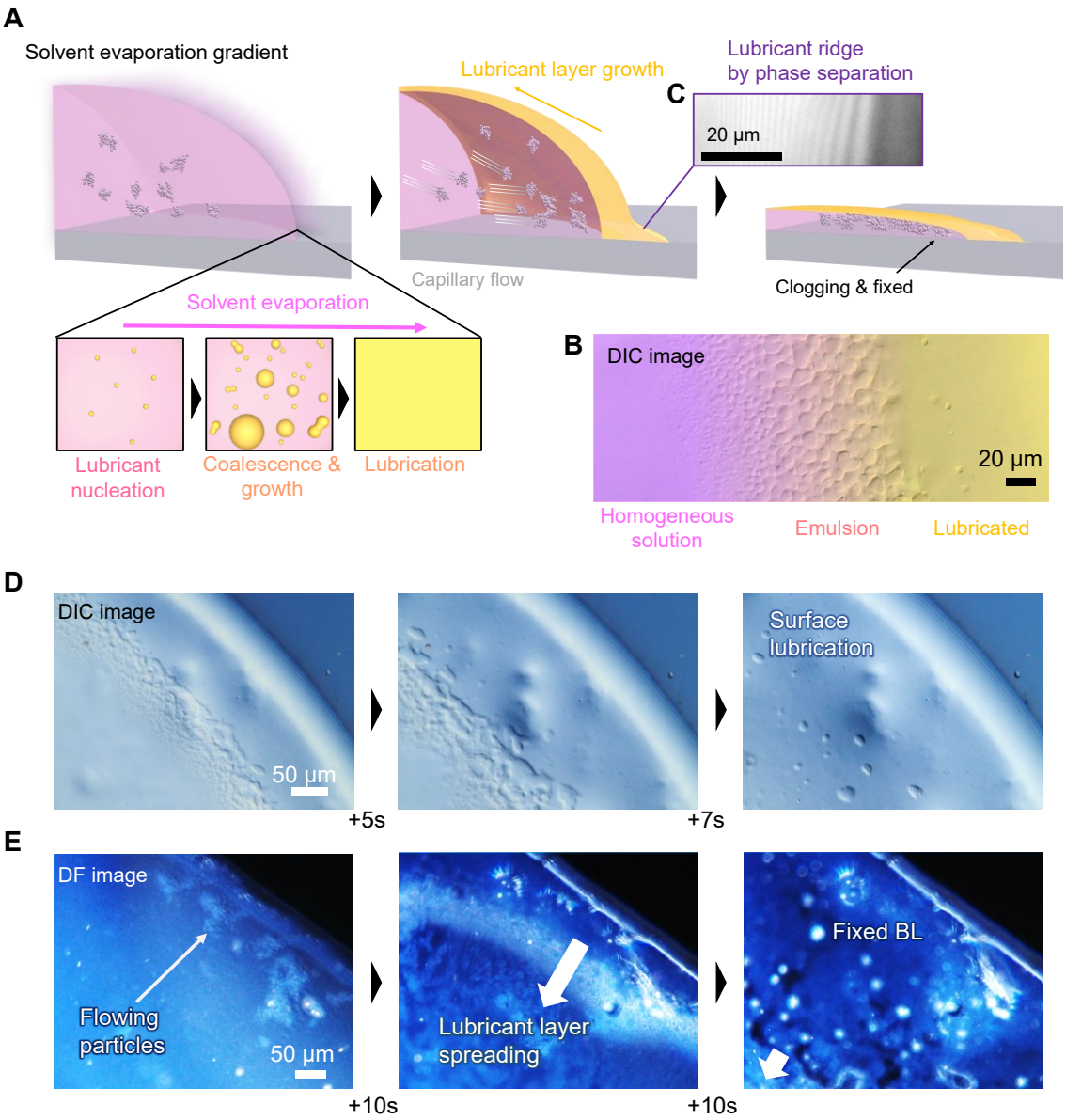

Figure 3. (A) Schematic of LIS formation dynamics. (B) Direct evidence of the LL formation from the homogeneous solution: with solvent evaporation, the lubricant droplets nucleate, grow, coalesce, and become the LL as observed by the differential interference contrast (DIC) observation. (C) The edge of the droplet observed by RICM. (D, E) Top-viewed time-lapsed microscopic images of a LIS formation when casting the coating solution on the glass substrate. (D) DIC observation, which shows LL formation on the outermost surface. (E) Dark field (DF) observation, which indicates particles aggregation behavior based on the scattering contrast.

2.3. Thermodynamic Stability of Omniphobic Lubricant Surface

Next, we evaluated the thermodynamic stability of the LIS by evaluating the wettability of the BL. The LL needs to be removed from the substrates to observe the microstructure of the BL. We utilized a supercritical drying process after solvent exchange because an ambient drying method would damage the BL structure (**Figure 4**A). We find the BL structure to be nanoporous and hierarchically roughened, as indicated in Figure 4B. The BL surface exhibits superhydrophobicity with static contact angle against water $\theta_s = 161.3°$ (Figure 4C) because the BL surface is uniformly covered with hydrophobic RTV silicone (Young contact angle for water is 112° [31]) as shown in Figure S10. Two criteria (Figure 4D) must be fulfilled to form a stable LL:[15]

$$\text{Criteria I: } S_{os(air)} \geq 0 \leftrightarrow \theta_{os(air)} = 0 \quad (1)$$

where $S_{os(air)}$ and $\theta_{os(air)}$ represent the spreading coefficient of the lubricant in air on the BL, and the static contact angle of lubricant in air on BL, respectively.

$$\text{Criteria II: } S_{os(tar)} \geq 0 \leftrightarrow \theta_{os(tar)} = 0 \quad (2)$$

where $S_{os(tar)}$ and $\theta_{os(tar)}$ represent the spreading coefficient of lubricant under the target liquid (to be repelled) on BL and the static contact angle of lubricant under the target liquid on BL, respectively. Criteria I indicates that the stable LL formation in air is fulfilled by $\theta_{os(air)} = 0$, as shown in Figure 4E. Criteria II indicates that the LL stability is in contact with other liquids as long as the liquids are immiscible with the lubricant; the liquid droplets that satisfy this condition slide off the stabilized LL. We confirm $\theta_{os(tar)} = 0$ under water (surface tension γ_{LV} = 72.8 mN m^{-1}), acetone (γ_{LV} = 23.3 mN m^{-1}), glycerol (γ_{LV} = 63.4 mN m^{-1}), or perfluoropolyether (γ_{LV} = 20.0 mN m^{-1}), as shown in Figure 4F; these liquid droplets slide off the LIS (Figure 4G and Movie S4). Ideally, to completely prevent the contact between BL and the target liquid, the disjoining pressure due to van der Waals interaction in the LL $\Pi(e)$, which is the pressure to resist the thinning of the LL thickness, had better be positive (i.e., $\Pi(e) > 0$, see section 4). [32] In this study, the disjoining pressure is positive for water, acetone, and perfluoropolyether, whereas it is negative for glycerol (Table S3).

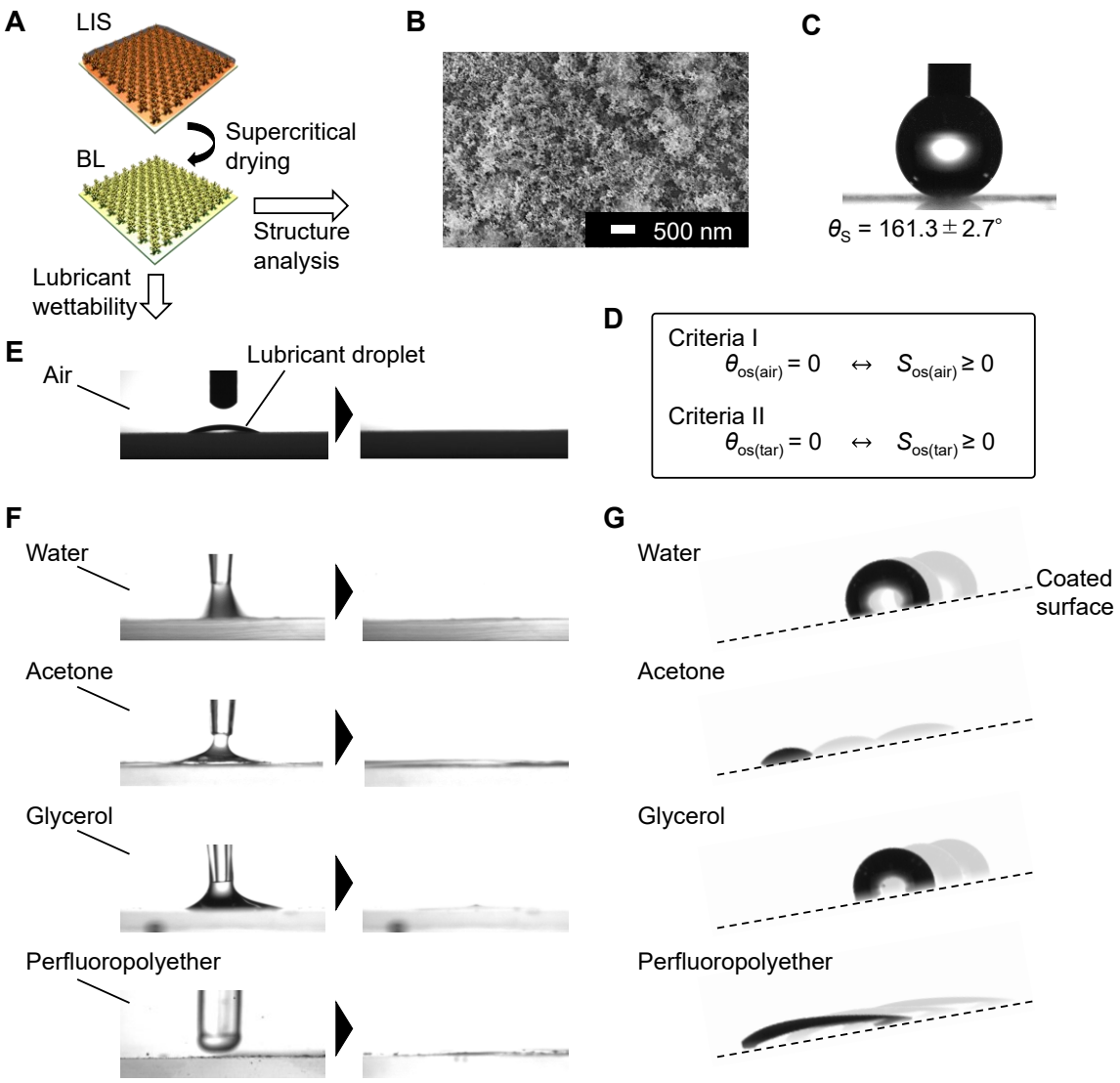

Figure 4. Thermodynamic stability of LIS. (A) Schematic to remove LL from the LIS by supercritical drying to obtain the BL surface for the wettability analysis. (B) Scanning electron microscopic (SEM) images of the BL. (C) Measurement of the static contact angle θ_s for a water droplet on the BL; the BL exhibits superhydrophobicity. (D) Two criteria to form a stable LL. Criteria I: A static contact angle of the lubricant in the air, $\theta_{os(air)} = 0$, is a necessary and sufficient condition for the spreading coefficient of the lubricant in the air, $S_{os(air)} \geq 0$; this implies the LL is stable in air. Criteria II: A static contact angle of the lubricant under target liquids, $\theta_{os(tar)} = 0$, is a necessary and sufficient condition for the spreading coefficient of the lubricant under target liquids $S_{os(tar)} \geq 0$; this implies the LL is stable under the target liquid as long as the liquids are immiscible with the lubricant. (E) Time-lapsed images of the lubricant droplet spread on the BL in the air. (F) Time-lapsed images of the lubricant droplet spreading on the BL under 4 different target liquids to be repelled. (G) The

thermodynamically stable omniphobicity of LIS tilting 10° against the 5 μL target liquid droplets fulfilling the criteria in (F).

2.4. Distinguishing Coating Solution from the Repelling Liquid

We used silicone oil as a lubricant, and it is stabilized on the structured surface of the RTV silicone whose chemical structure is similar to that of the lubricant. Thus, interfacial tension between the RTV silicone and silicone oil is negligible. In this case, the liquid repellency of LIS depends on the miscibility of the LL and the target liquids. Meanwhile, the one-step LIS formation relies on the LL formation from the homogeneous solution, which indicates that the solvent of the coating solution needs to be miscible with the lubricant. We calculated the Hansen solubility parameter (HSP) for the lubricant to estimate the liquid−lubricant miscibility, as shown in **Figure 5**A (See Table S4-S5, Figure S11). The HSP is a value used to predict the miscibility of the two different substances, and it is based on the concept of the "like dissolves like" consideration. The HSP, defined as the square root of cohesive energy density of a substance, is divided into three independent numeric values: dispersion force term (δD), polarity term (δP), and hydrogen bonding term (δH). Two different substances can be miscible when the HSP of the substances in the three-dimensional space of δD, δP, and δH are close. The followings are the detailed criteria for the HSP analysis:[33]

$$\text{Miscible: } (\delta D_{sol} - \delta D_{lub})^2 + (\delta P_{sol} - \delta P_{lub})^2 + (\delta H_{sol} - \delta H_{lub})^2 \leq R_{lub}^2 \quad (3)$$

and

$$\text{Immiscible: } (\delta D_{sol} - \delta D_{lub})^2 + (\delta P_{sol} - \delta P_{lub})^2 + (\delta H_{sol} - \delta H_{lub})^2 > R_{lub}^2 \quad (4)$$

where δD_{sol}, δP_{sol}, and δH_{sol} represent the dispersion, polar, and hydrogen bonding components of the test solvents in the HSP, respectively. δD_{lub}, δP_{lub}, and δH_{lub} represent the center coordinate, and R_{lub} represents the radius of the Hansen sphere of the lubricant. The lubricant miscible liquids are placed within the range of the Hansen sphere, which cannot be repelled by the LIS; however, they can be used for the coating solution as long as it is volatile. Meanwhile, the lubricant immiscible liquids are placed out of the range of Hansen sphere, which can be repelled by the LIS using this lubricant. This classification is independent of the surface tension of the liquids. Figure 5B shows that the measured contact angle hysteresis θ_{hys} of the various liquids. The immiscible liquids with the surface tension range of γ_{LV} = 20.0–72.8 mN m^{-1} is repelled with a limited θ_{hys}, as shown in Figure 5C. However, for isopropanol (γ_{LV} = 21.8 mN m^{-1}), hexadecane (γ_{LV} = 28.2 mN m^{-1}), or toluene (γ_{LV} = 28.5 mN m^{-1}), the liquids wet the LIS. Figure 5D shows a hemi-wicked isopropanol that exhibits the receding contact angle of ~ 0° with a decrease in the volume of the cast isopropanol on the LIS (Figure S12). Based on this analysis, we replace the lubricant and/or solvent to others and confirm the

LIS formation; its function requires both the solvent–lubricant miscibility and the lubricant–target liquid immiscibility (Table 1).

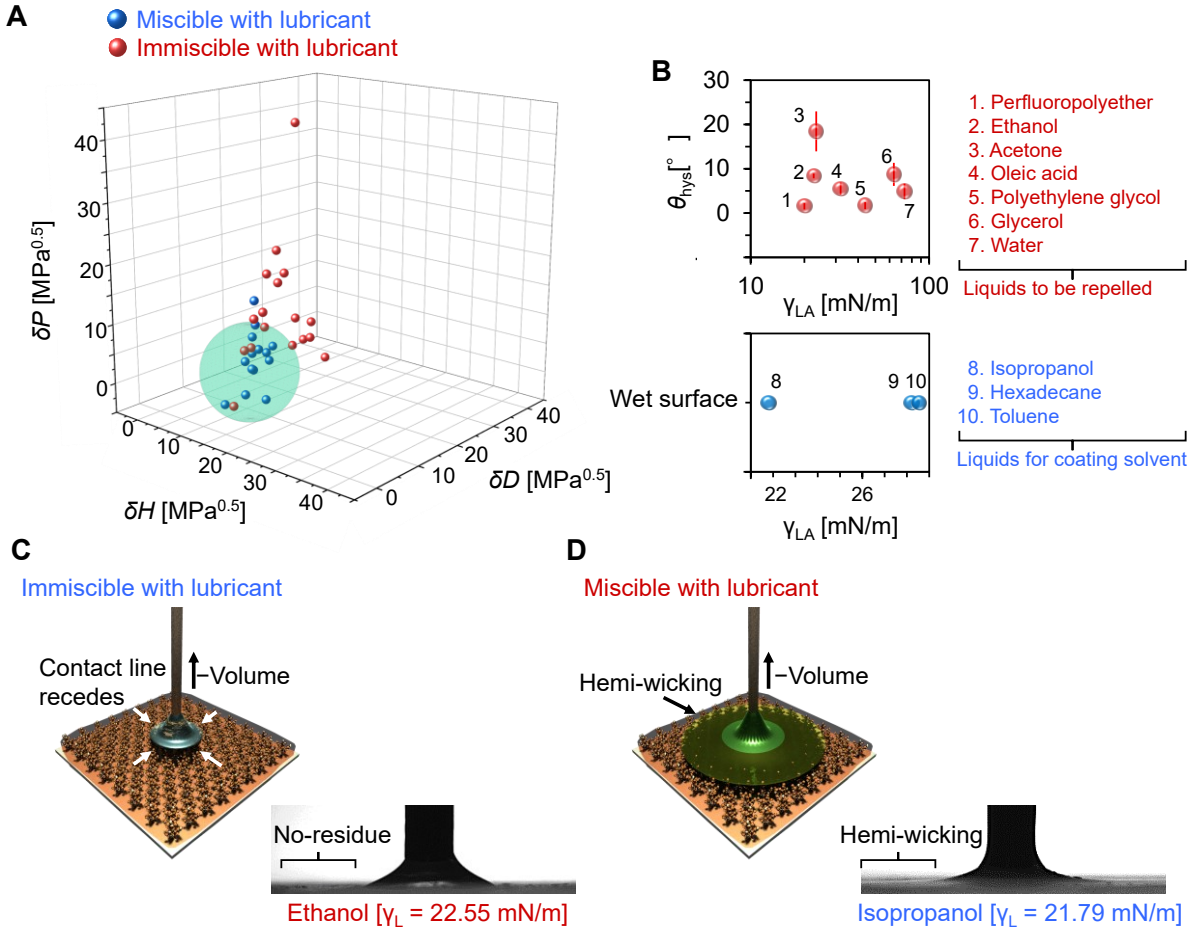

Figure 5. (A) Lubricant miscibility analysis using the Hansen solubility parameter (HSP) for the lubricant. Blue sphere: solvent miscible with the lubricant; Red sphere: solvent immiscible with the lubricant; and Green sphere: Hansen sphere of the lubricant. (B) Contact angle hysteresis θ_{hys} of various liquids with different surface tension γ_{LV}. Class of liquids immiscible with the lubricant that can be repelled on the LIS (C). Liquids miscible with the lubricant wet the LIS (D) and can be used for coating the solvent as long as it is volatile.

Table 1. Influence of solvent–lubricant–target liquid miscibility on liquid repellency.

Solvent	Lubricant [a)]	Target liquid	Are the solvent and lubricant miscible? [c)]	Are the lubricant and target liquid immiscible? [c)]	Does a 5 μL target liquid droplet slide off with a 10° tilting?
Isopropanol	Silicone oil (10 cSt)	Water	Yes	Yes	Yes
Isopropanol	Silicone oil (100 cSt)	Water	Yes	Yes	Yes
Isopropanol	Oleic acid [b)]	Water	Yes	Yes	Yes
Isopropanol	Perfluoropolyether [b)]	Water	No	Yes	No
Isopropanol	Liquid paraffin [b)]	Water	No	Yes	No
Isopropanol	Polyethylene glycol [b)]	Water	Yes	No	No
Hexane	Silicone oil (10 cSt)	Water	Yes	Yes	Yes
Ethanol	Silicone oil (10 cSt)	Water	Yes	Yes	Yes
Dichloropentafluoropropane	Silicone oil (10 cSt)	Water	Yes	Yes	Yes
Water	Silicone oil (10 cSt)	Water	No	Yes	No
Isopropanol	Silicone oil (100 cSt)	Perfluoropolyether	Yes	Yes	Yes
Isopropanol	Silicone oil (100 cSt)	Ethanol	Yes	Yes	Yes
Isopropanol	Silicone oil (100 cSt)	Acetone	Yes	Yes	Yes
Isopropanol	Silicone oil (100 cSt)	Oleic acid	Yes	Yes	Yes
Isopropanol	Silicone oil (100 cSt)	Polyethylene glycol	Yes	Yes	Yes
Isopropanol	Silicone oil (100 cSt)	Glycerol	Yes	Yes	Yes
Isopropanol	Silicone oil (100 cSt)	Isopropanol	Yes	No	No
Isopropanol	Silicone oil (100 cSt)	Hexadecane	Yes	No	No
Isopropanol	Silicone oil (100 cSt)	Toluene	Yes	No	No
Isopropanol	Silicone oil (10 cSt)	Acetone	Yes	No	No
Isopropanol	Silicone oil (10 cSt)	Oleic acid	Yes	No	No
Isopropanol	Silicone oil (10 cSt)	Ethanol	Yes	No	No
Isopropanol	Silicone oil (10 cSt)	Glycerol	Yes	Yes	Yes

[a)] $\Phi_{lub} = 0.28$. [b)] When the lubricant is not silicone oil, the thermodynamic stability as examined in Section 2.3 is not guaranteed. [c)] Judged from the solubility test. The experimental procedure is indicated in Hansen Solubility Parameter section in detail.

2.5. Influence of the Lubricant Fraction on Water Repellency

Next, we studied the effect of the lubricant fraction Φ_{lub} on the wettability of the coated surfaces; the results are shown in **Figure 6**. For varying values of Φ_{lub}, four interfacial states are observed as shown in Figures 6A–D. For $\Phi_{lub} < 0.01$, lubricant hardly appears to the surface, and the BL is exposed. Thus, the coated surface exhibits superhydrophobicity $\theta_s = \sim 150°$; however, the cast water droplet sticks to the few lubricated spot on the surface (Figure 6A) and the sliding angle α increases with Φ_{lub} (Figure 6E). For $\Phi_{lub} > 0.01$, the interfacial state transitions from the superhydrophobic to the slippery state (Figure 6B). In this range, lubricant partially covers the BL; thus, the stick-slip motion of the water droplet is observed. For $0.09 < \Phi_{lub} < 0.91$, the coated surface becomes the LIS (Figure 6C, Figure S13) and exhibits $\theta_s = \sim 110°$, which is constant with Φ_{lub}, and a negligibly low α owing to the slippery lubricant−water interface (Figure 6E). For $\Phi_{lub} > 0.91$, the water droplet sticks to the coated surface, and the droplet does not slide off the surface because the sparse BL fails to stabilize LL as a water droplet that is in direct contact with the bare glass substrate (Figure 6D).

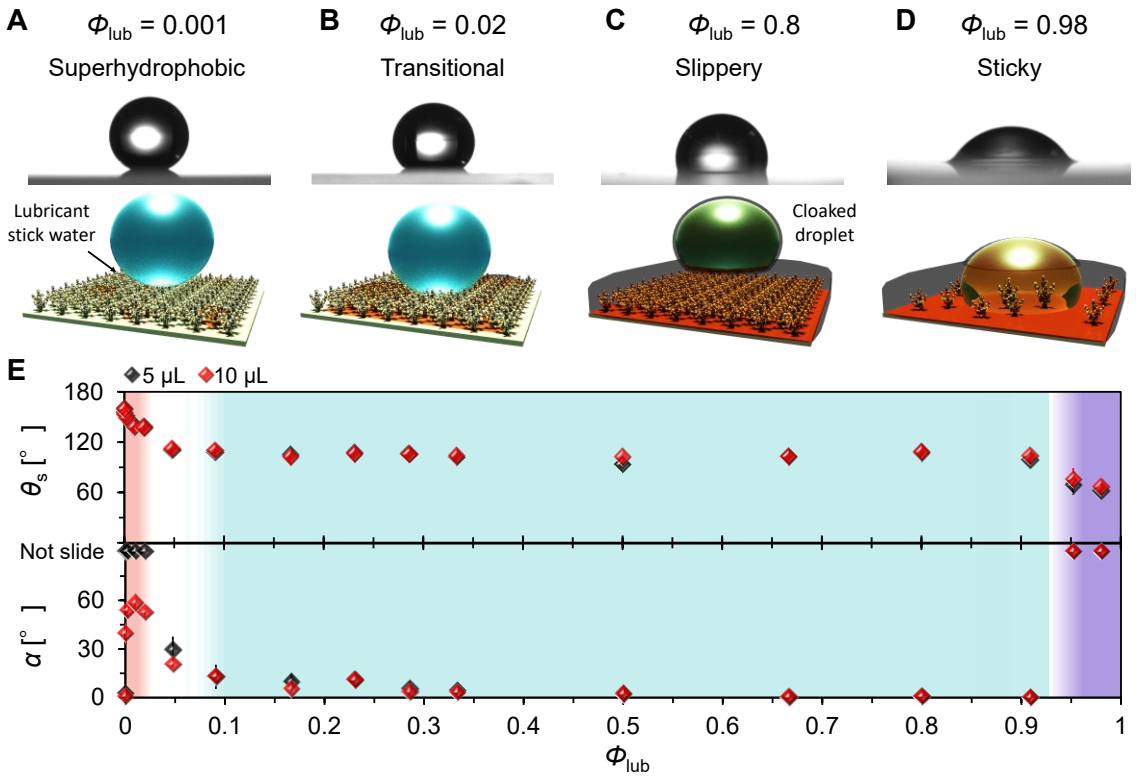

Figure 6. Wettability transition as a function of the lubricant fraction in the coating solution Φ_{lub}. (A-D) Side view photographs and schematics of the water droplet contacting the LIS with different Φ_{lub}. Four interfacial states are observed with varying Φ_{lub}: superhydrophobic state (A), transitional state between the superhydrophobic and slippery states (B), slippery

state (C), and sticky state (D). (E) θ_s and sliding angle α for 5 or 10 μL water droplets as a function of Φ_{lub}. Red area: sticky superhydrophobic area except for the case $\Phi_{lub} = 0$; light blue area: slippery state; and purple area: sticky state by droplet contacts with sparse BL.

2.6. Emergence of Transparency

The optical transparency of coated surfaces with a varied Φ_{lub} is shown in **Figure 7**A. For $\Phi_{lub} < 0.09$, transmittance T decreases with an increase in Φ_{lub}. This result indicates that the inhomogeneity of the structure inside the coating (Figure 7B) becomes large because the absorption of the dispersion is negligibly small; this is supported by weakening of the wavelength dependence on T with an increase in Φ_{lub}. For $\Phi_{lub} > 0.09$, T remains mostly constant with λ, which indicates the surface is fully covered with LL (Figure 7C) and the scattering is minimized by surface homogeneity.[34] Consequently, the coated surface exhibits $T = \sim 90\%$ at this λ, which is almost the same as the one on the uncoated glass substrate (Figure S15).

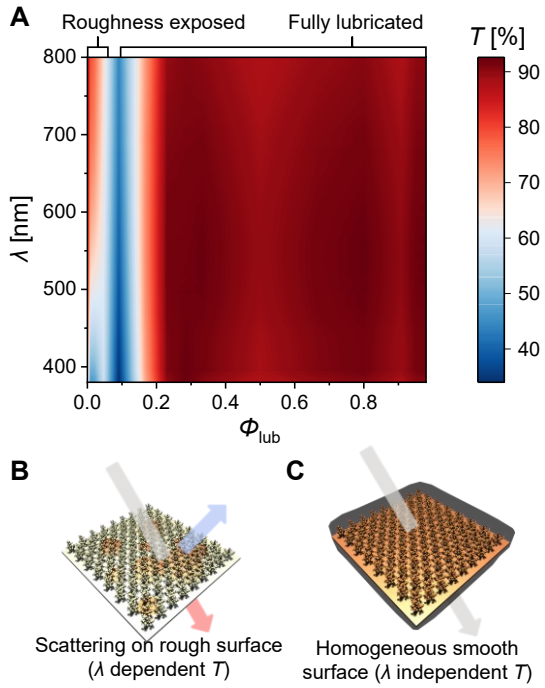

Figure 7. (A-C) Wavelength (λ) dependent transmittance (T) analysis of the coated glass substrate with different Φ_{lub} values. (A) T mapping as a function of Φ_{lub} and λ. (B) Schematics of roughness exposed coated surfaces at $\Phi_{lub} < \sim 0.09$. (C) Schematics of fully lubricated coated surface at $\Phi_{lub} > \sim 0.09$. The scattering is minimized at these atomically smooth surfaces.

2.7. Damage Torelance

The LIS kept liquid slipperiness after cutting and abrasion (**Figure 8**A and Movie S6). The robustness of the LIS coating was characterized by the abrasion test (Figure 8B and Figure

S16 for the experimental setup). The static and dynamic friction constants exhibited mostly plateau values of 0.3 till 900 times abrasions for the LIS by silicone oil (10cSt). However, these values suddenly increased to 0.9 for static friction constant and 0.7 for dynamic one, which is comparable to that on the glass substrate. Thus, the BL broke and the glass substrate was exposed after 1000 times abrasions. The breakage in BL deteriorates the liquid-repellency as confirmed by the variation in receding contact angles decreased from 106° to 78° after the abrasion test (Figure 8C). While this, the friction constants exhibited a plateau value of 0.1 for the LIS by silicone oil (100cSt). It indicates that the LIS coating is mechanically stable after the abrasion test. The coating maintained the advancing and receding contact angles even after 1000 times abrasions. The difference in friction constants between the LISs with different silicone oil viscosity comes from the coating thickness below the abrasive which decreases with the invasion depth in the abrasive inside the LL (see Figure S17). The coating for the LIS by silicone oil (100cSt) is thicker than that by silicone oil (10cSt). Landau–Levich–Derjaguin law explains this: [32, 35]At constant surface energy of the lubricant and constant abrasion speed, the coating thickness below the abrasive is increased with lubricant viscosity. Since the surface slipperiness increased with the coating thickness, the friction constants of the coating with silicone oil (100 cSt) were lower than that with silicone oil (10 cSt). Moreover, the LIS exhibited a self-repairing property (Figure 8D) against cutting when the surface is fully covered with LL. The LL is stable against shear stress because of the constant sliding angle (Figure 8E).

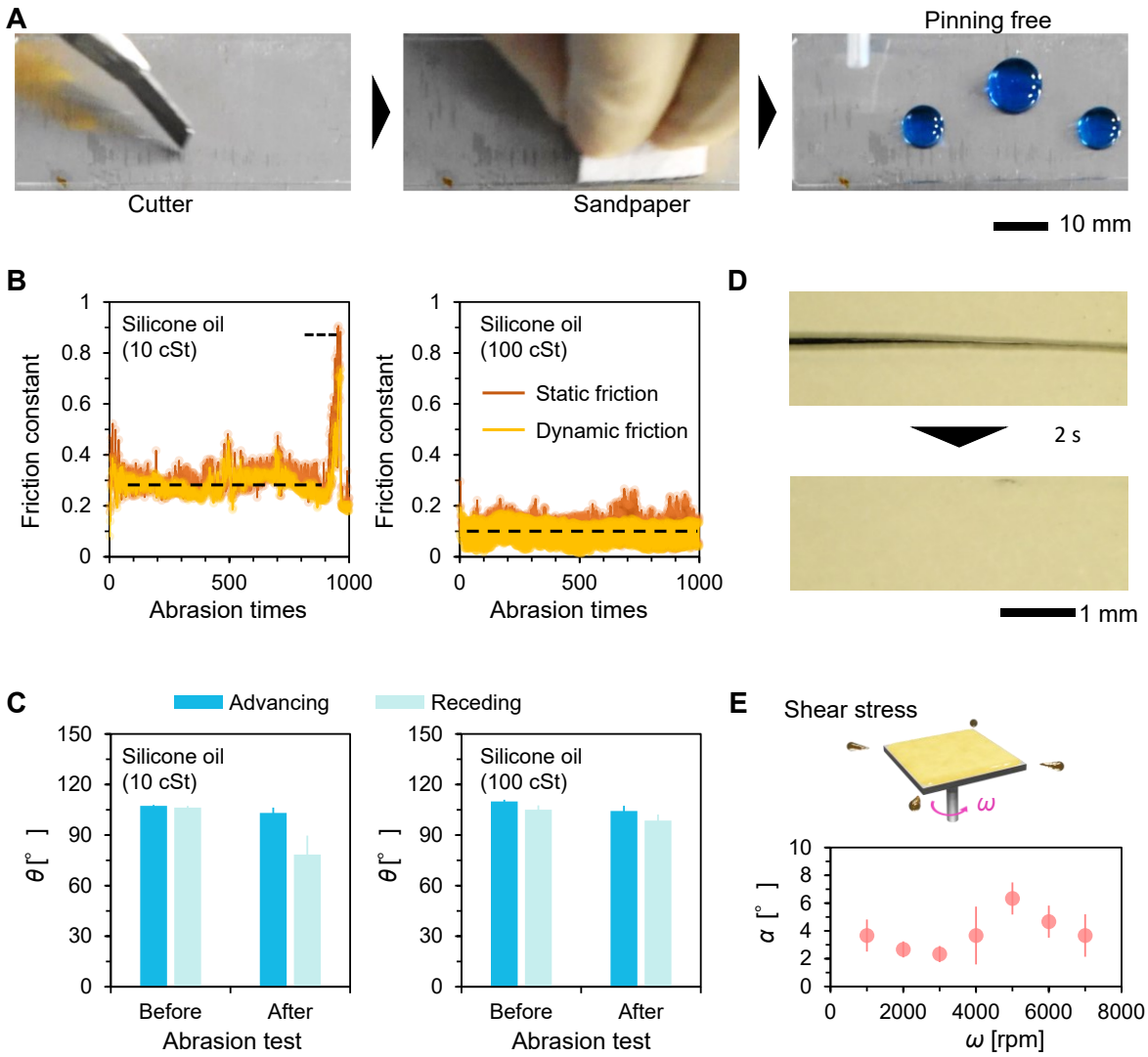

Figure 8. (A) Cutting and abrasion resistance of the coating. (B, C) The influence of abrasion times on (B) static and dynamic friction constants, and (C) advancing and receding contact angles. Silicone oil (10 cSt) and silicone oil (100 cSt) are used as the LL. (D) Photographs of the coated surface with $\Phi_{lub} = 0.28$ just after scratching and after 10 s. The coated surfaces exhibit a self-repairing property at the fully lubricated regions. (E) Sliding angle of a 5 μL water droplet after adding shearing stress up to 7000 rpm for 300 s.

2.8. Application: Car Window Coating and Outdoor Stability

We finally show this coating with scalability, surface liquid-repellency, transparency, and self-repairing functions that can be applied to the car coating as a potential application. **Figure 9**A-B shows the coating solution sprayed on a hydrophilic car window (Movie S5). After the coating, the window retains its transparency and repels water droplets even when the car is stationary (Figure 9A); commercially available hydrophobic car coatings require wind or inertial pressure to remove the water when the car is in motion. After drying, the uncoated car window exhibit fouling caused by the evaporated residual water droplets, whereas the coated surface remains clean (Figure 9B). In this application, the coating encounters mist, wind pressure, and dust accumulation. The LIS exhibited slipperiness to water mist applied by hand-spraying (Figure 9C, and Movie S7). This result indicates the LIS is stable against micro-sized water. We also confirmed the LIS can repel hot water (Figure S18 and Movie S8) while superhydrophobic surface suffers from the repellence. [REF] Moreover, the LIS kept water repellency after nitrogen gas blowing (Pressure: 0.2MPa; Blowing distance: 100 mm; Blowing angle: 45° ; Blowing time: 30 min.) which can be seen in Figure 9D and Movie S9. Figure 9E (and Movie S10) shows the self-cleaning property of the LIS. Therefore, the LIS coating is promising for the outdoor applications. These functions work as long as the LL is stable.

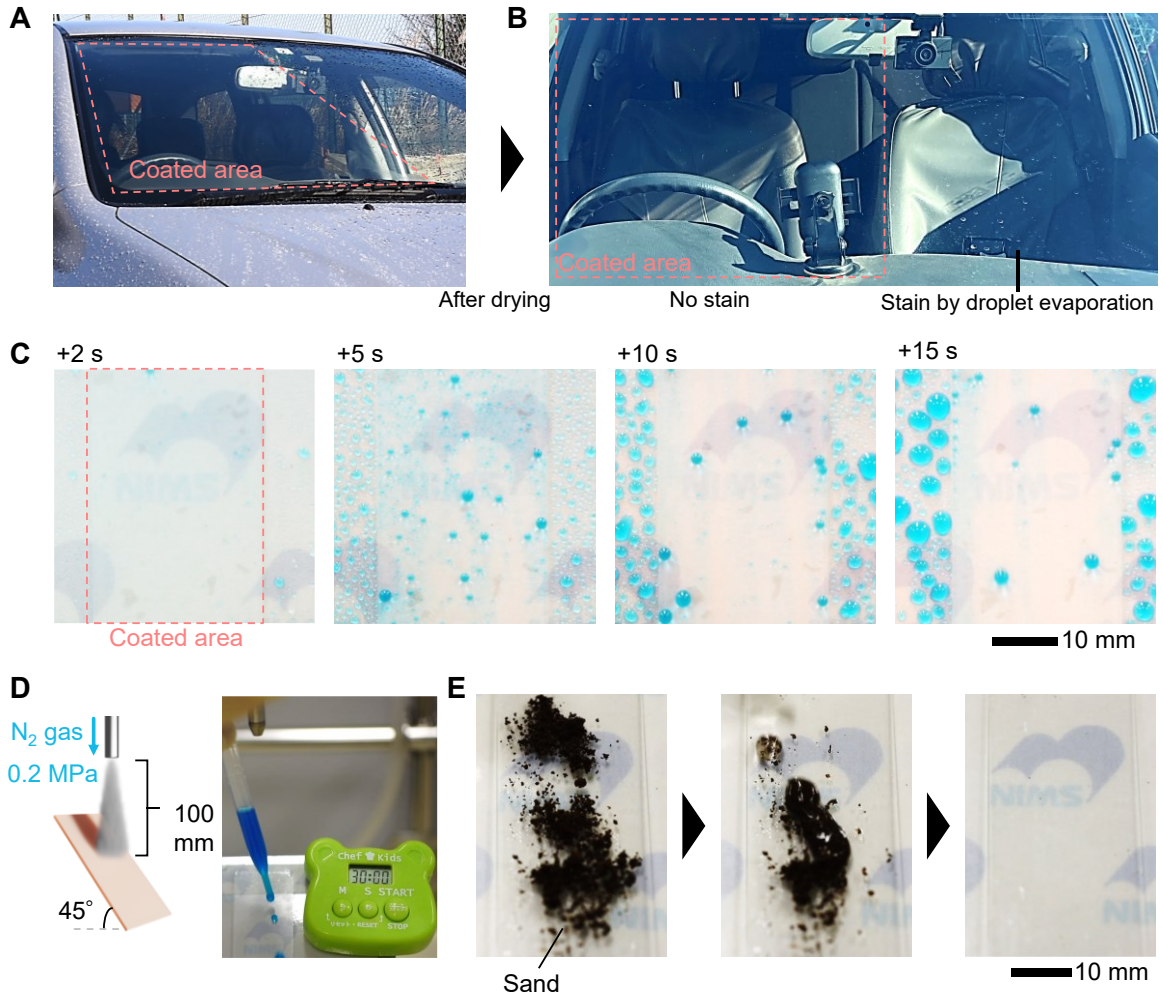

Figure 9. (A, B) Application of the large-scale LIS coating to the anti-fouling car window. The half-area of the car window is coated with the LIS by spraying the coating solution and (A) observed water shower adhesion behavior. (B) Photograph of the car window captured outside, after the window is dried in the sun. The LIS-coated area exhibits an anti-fouling property, whereas the uncoated window exhibits stains. (C) Anti-mist performance. Misty water was sprayed several times on the vertically set coating. (D) Anti-wind performance. Nitrogen gas was continuously blown to the 45 tilted coating for 30 min. Then, the water repellency was retained. (E) Self-cleaning procedure of the coating. Water droplets remove sand covering the coating.

3. Conclusion

In this study, a versatile coating solution was used to create LIS on solid substrates by a simple scalable process. The LIS was obtained through solvent evaporation induced dual layer formation using the dynamic capillary clogging of the BL and the ouzo-like surface LL spreading. The possible coating combinations can be expanded based on the thermodynamic stability condition and the HSP estimation, which are available for general LIS formation. The LIS can be commercialized by supplementing it with our coating solution because it is scalable, one-step, and its surface is transparent, omniphobic, and self-repairing. Another advantage of this process is the facile tuning of the coating thickness as the LIS is formed by a treatment-free single-step wet process (generally, LL thickness can only be controlled by laboratory-scale shearing stress). Moreover, very thin LIS may be used in heat transfer processes. However, thick coatings can improve the long-term stability of the coating as coating damage cannot be avoided. This study will advance the commercial and scientific use of LIS for further potential applications as the LIS coating becomes more versatile and generally available. From the viewpoint of the commercial products, A superhydrophobic surface is commercially available and it is spread using a disposable coating solution; [36, 37] therefore, supplying a coating solution to form the LIS appears to be a promising approach to realizing practical applications. We believe this work will help the commercialization of LIS and further industrial applications because the LIS coating is versatile and can be made commercially available.

4. Experimental Section

Materials: All reagents were used as received. Fumed nanoparticles (AEROSIL® RX 200, AEROSIL® RX 50, AEROSIL® RX 300, AEROSIL® OX 50, AEROSIL® 200, AEROXIDE® Alu 65, AEROXIDE®TiO2 NKT90) were procured from Evonik industries, Germany. Colloidal nanoparticles (QSG-10, QSG-30, QSG-100) were obtained from Shin-Etsu Chemical Co., Ltd., Japan. Binder DOWSIL™ HC 2100 and SYLGARD™ 184 Silicone Elastomer Kit were purchased from Dow Inc., USA. Silicone oil (10 cSt) DMS-T11 was purchased from Gelest. Silicone oil (100 cSt) ASO-100 was purchased from AS ONE Corp., Japan. Oleic acid, liquid paraffin, Polyethylene glycol PEG 400, 1,4-Dioxane (99.5%), 2-phenoxy ethanol (99.0%), acetone (99.5%), acetonitrile (99.5%), chloroform (99.0%), dimethyl sulfoxide (99.0%), dipropylene glycol (95.0%), ethyl acetate (99.5%), gamma butyrolactone (99.0%), hexadecane (97.0%), hexane (96.0%), isopropanol (99.7%), methanol (99.5%), propylene carbonate (98.0%), tetrahydrofuran (99.0%), toluene (99.5%), and Nile red were purchased from Wako Pure Chemical Industries, Ltd., Japan. 1-Butanol (99.5%), cyclohexane (98.0%), cyclohexanol (99.0%), diethylene glycol (99.0%), methyl ethyl ketone (99.0%), *n*-butyl acetate (99.0%), *N*-methyl pyrrolidone (99.5%), propylene glycol monomethyl ether acetate (98.0%), and tetrachloroethylene (99.0%) were purchased from Nakalai Tesque, Japan. Perfluoropolyether Krytox GPL-103 was purchased from The Chemours company, USA. Glycerol, Di-(2-ethylhexyl)azelate (75.0%), diacetone alcohol (98.0%), methyl isobutyl ketone (99.5%), and propylene glycol monomethyl ether (98.0%) were obtained from TCI, Japan. Dimethyl formamide (99.5%), ethanol (99.9%), methylene dichloride (99.5%) were purchased from Kanto Chemical Co., Inc., Japan. Dichloropentafluoropropane Asahiklin® AK-225 was purchased from AGC Inc., Japan. Ultrapure water (resistivity: 18.2 MΩ·cm) was obtained using the Direct-Q®UV3 system from Merck KGaA, Germany.

Coating Solution: Unless specified, we used the mixture of 0.08 g hydrophobic fumed silica nanoparticles (AEROSIL® RX 200), 0.04 g silicone binder (DOWSIL™ HC 2100), 5 mL isopropanol, and 2 mL silicone oil (Φ_{lub} =0.28). For the silicone oil, we confirmed that the water contact angle and sliding angle are not different for DMS-T11 and ASO-100. The difference is solvent miscibility (Table S5) and lubricant mobility (water sliding speed). [32] Thus, DMS-T11 is used for the water repelling coating while ASO-100 is used for the omniphobic coating. The mixture is stirred for at least 12 h to obtain a coating solution. The coating solution is coated onto a glass substrate (size: 1.0 × 26 × 76 mm, Muto Pure Chemicals Co., Ltd., Japan) using a dip coater (DT-0001-S3, SDI Company Co., Ltd,

withdrawing speed is 9 mm s^{-1}), and it is dried in the ambient condition for 10 min. For this condition, the coating thickness is 25.6±3.1 μm (n = 3). Commercially available substrates, and aluminum, polycarbonate, and nitrile rubber plates were used. Spray coating was performed but not quantified because it was performed using a commercial hand spray bottle.
Supercritical Drying: The substrates were immersion-washed in hexane for 24 h to remove the LL. Then, supercritical CO_2 drying was performed at 40 °C and 10 MPa using SYGLCP-81 (Sanyu Gijutsu Co., Ltd., Japan).
Digital Microscopy: Digital microscopic observations with DIC, DF, and BF modes were conducted using DSX-1000, Olympus Corporation, Japan.
Wettability Analysis: Static contact and sliding angles were measured using a contact angle meter (Drop master-SA-301, Kyowa Interface Science Co., Ltd., Japan). The volume of the probe liquid was 5 μL, if not stated otherwise. Advancing and receding contact angles were measured by increasing and decreasing the volume of water on the test surface.
Hansen Parameter: The lubricant and 30 types of test organic solvents were individually mixed, and the miscibility was carefully evaluated manually (Table S4). The solubility of the two liquids (lubricant and organic solvent) was checked according to the following procedure. The 100 μL lubricant and the 100 μL test organic solvents were individually loaded into a transparent microtube and then applied vigorous shaking with a vortex mixer. The two liquids' miscibility was finally judged from the direct observation by naked eyes. The results were then investigated using the HSPiP program (ver. 5.3.06) developed for HSP estimation from the miscibility test (Table S5). With prior knowledge of the HSP of the test solvents, the program can suitably estimate the center coordinate and radius of the Hansen sphere of the target lubricants. The test solvents were selected because the HSP of the 30 organic solvents were well-dispersed in the HSP three-dimensional space which manifest the reliable estimation of the HSP.
Reflection Interference Contrast Microscopy (RICM): Figure S9A shows a schematic of the developed RICM. [35] A Köhler illumination is implemented using white light LED (MCWHLP1, Thorlabs), four lenses, and two irises to realize homogeneous illumination. The reflection of the incident light at the beam splitter was eliminated using cross polarizers combined with an achromatic quarter-wave plate (EKSMA Optics). The sample liquid is placed on a cover glass and illuminated by an objective lens (CF Plan 50× NA 0.80, Nikon). Reflection inside the objective lens was negligibly small. The reflected light was focused on a CMOS camera (CHU30-B-RS, Shodensha) after passing through a bandpass filter (center

wavelength: 532 nm, full width half maximum: 10 nm, FL532-10, Thorlabs) to monochromate the reflected light. The frame rate of the CMOS camera was set to 50 fps.

The edge of the droplet observed by the RICM is shown in Figure 2B. The image shows the intensity variation that originates from the interference of the light reflected at the cover glass/oil interface I_1, and the oil/air interface I_2. The net intensity I is expressed as

$$I=I_1+I_2+2(I_1I_2)^{0.5}\cos(2kh+\pi) \quad (5)$$

where k denotes the magnitude of the wavevector of light in the oil and h represents the thickness of the oil. In this formulation, we neglect the effect of the illumination numerical aperture and the curvature of the interfaces that result in a decreased contrast. The evaluation of h was performed by obtaining the local maximum value of I as a function of time and the horizontal position. The temporal variation of h as a function of the horizontal position is shown in Figure S9B. We successfully determined the temporal variation of the edge shape during the coating; the edge shape shows a wetting ridge at all times, and it is a direct evidence of phase separation (Figure S9C).

Disjoining pressure: To completely prevent the contact between BL and the target liquid, disjoining pressure due to van der Waals interaction in the LL $\Pi(e)=A/(6\pi e^3)$, where A is Hamaker constant and e is LL thickness, has better be positive, that is, $A>0$. [29] Here, A is estimated as:

$$A = \frac{3}{4}k_BT\left(\frac{\epsilon_o-\epsilon_{tar}}{\epsilon_o+\epsilon_{tar}}\right)\left(\frac{\epsilon_s-\epsilon_o}{\epsilon_s+\epsilon_o}\right)+\frac{3h\nu_e}{8\sqrt{2}}\frac{(n_s{}^2-n_{tar}{}^2)(n_s{}^2-n_o{}^2)}{\sqrt{(n_s{}^2+n_o{}^2)(n_{tar}{}^2+n_o{}^2)}\left[\sqrt{n_{tar}{}^2+n_o{}^2}+\sqrt{n_s{}^2+n_o{}^2}\right]} \quad (6)$$

where k_B is the Boltzmann constant, T is the absolute temperature, h is the Planck constant, $\nu_e \approx 4\times10^{15}$ s^{-1} is the plasma frequency of free electron gas, while $\varepsilon_{s/o/tar}$ and $n_{s/o/tar}$ are the dielectric constants and refractive indexes of the BL, LL, and target liquid, respectively. The calculated results are summarized in Table S3.

Other Characterizations: The optical measurement was conducted using an ultra violet-visible spectrophotometer (UV-Vis V-770) from the JASCO Corporation, Japan. Surface structures and elemental mappings of the supercritical dried LIS were observed using field emission SEM (SU8230, Hitachi, Ltd., Japan) and energy dispersive X-ray (EDX) spectroscopy from HORIBA, Ltd., Japan. Surface roughness was measured using laser microscopy performed with OLS5100 (Olympus Corporation, Japan). A shearing test was

conducted using spin-coater ACT-220AII from Active Ltd., Japan. The water contents in the solvent were confirmed using the Karl Fischer moisture measurement system MKC-710M from Kyoto Electronics Manufacturing Co., Ltd. The sample photographs were captured using a digital camera (D-5600, Nikon Corporation, Japan).

Statistics: The experimental data were obtained for statistical significance. The data were plotted using Microsoft Excel or Origin Pro and presented by mean ± SD with a sample size of at least $n = 3$. A droplet transportation velocity inside the silicone tube is obtained by the image analysis of the movie S2.

Supporting Information

Supporting Information is available from the Wiley Online Library or from the author.

Acknowledgements

The authors acknowledge Makiko Yabune who supported this work, Dr. Masanobu Naito for the use of abrasion tester, and Dr. Toshihiko Mandai who helped the determination of the water content in the solvent. This work was supported by WPI-MANA and ICYS. M.T. acknowledges the support from JSPS KAKENHI No. 21H01643, and JSPS LEADER. T. U. acknowledges the support from JSPS KAKENHI No. 20H02804, and 20K21229. M.T. conceived the research, designed the experiments, and wrote the paper. M.T. and G.H. prepared the sample. M.T., G.H., T. H., and T. U. analyzed the data and discussed the results. M.T. is responsible for all the data.

Received: ((will be filled in by the editorial staff))
Revised: ((will be filled in by the editorial staff))
Published online: ((will be filled in by the editorial staff))

References

[1] A. Dhyani, J. Wang, A. K. Halvey, B. Macdonald, G. Mehta, A. Tuteja, *Science* **2021**, *373*, 294.

[2] A. Y. Fadeev, T. J. McCarthy, *Langmuir* **1999**, *15*, 3759.

[3] J. Liu, Y. Sun, X. Zhou, X. Li, M. Kappl, W. Steffen, H. J. Butt, *Adv. Mater.* **2021**, *33*, 202100237.

[4] L. Feng, S. Li, Y. Li, H. Li, L. Zhang, J. Zhai, Y. Song, B. Liu, L. Jiang, D. Zhu, *Adv. Mater.* **2002**, *14*, 1857.

[5] Z. Dong, M. Vuckovac, W. Cui, Q. Zhou, R. H. A. Ras, P. A. Levkin, *Adv. Mater.* **2021**, *33*, 202106068.

[6] M. Tenjimbayashi, S. Samitsu, Y. Watanabe, Y. Nakamura, M. Naito, *Adv. Funct. Mater.* **2021**, *31*, 2010957.

[7] A. K. Kota, Y. Li, J. M. Mabry, A. Tuteja, *Adv. Mater.* **2012**, *24*, 5838.

[8] K. Golovin, D. H. Lee, J. M. Mabry, A. Tuteja, *Angew. Chem. Int. Ed.* **2013**, *52*, 13007.

[9] T. Liu and C.-J. Kim, *Science*, **2014**, *346*, 1096.

[10] T. Verho, J. T. Korhonen, L. Sainiemi, V. Jokinen, C. Bower, K. Franze, S. Franssila, P. Andrew, O. Ikkala, R. H. A. Ras, *Proc. Natl. Acad. Sci. USA* **2012**, *109*, 10210.

[11] A. K. Kota, G. Kwon, A. Tuteja, *NPG Asia Mater.* **2014**, *6*, e109.

[12] W. Xu, H. Zheng, Y. Liu, X. Zhou, C. Zhang, Y. Song, X. Deng, M. Leung, Z. Yang, R. X. Xu, Z. L. Wang, X. C. Zeng, Z. Wang, *Nature* **2020**, *578*, 392.

[13] T. S. Wong, S. H. Kang, S. K. Y. Tang, E. J. Smythe, B. D. Hatton, A. Grinthal, J. Aizenberg, *Nature* **2011**, *477*, 443.

[14] M. Tenjimbayashi, R. Togasawa, K. Manabe, T. Matsubayashi, T. Moriya, M. Komine, S. Shiratori, *Adv. Funct. Mater.* **2016**, *26*, 6693.

[15] J. D. Smith, R. Dhiman, S. Anand, E. Reza-Garduno, R. E. Cohen, G. H. McKinley, K. K. Varanasi, *Soft Matter* **2013**, *9*, 1772.

[16] M. Villegas, Y. Zhang, N. Abu Jarad, L. Soleymani, T. F. Didar, *ACS Nano* **2019**, *13*, 8517.

[17] S. Sett, X. Yan, G. Barac, L. W. Bolton, N. Miljkovic, *ACS Appl. Mater. Interfaces* **2017**, *9*, 36400.

[18] L. Chen, S. Park, J. Yoo, H. Hwang, H. Kim, J. Lee, J. Hong, S. Wooh, *Adv. Mater. Interfaces* **2020**, *7*, 2000305.

[19] X. Gou, Z. Guo, *Langmuir* **2020**, *36*, 8983.

[20] X. Yao, S. S. Dunn, P. Kim, M. Duffy, J. Alvarenga, J. Aizenberh, *Angew. Chem. Int. Ed.* **2014**, *53*, 4418.

[21] Y. Zhuo, F. Wang, S. Xiao, J. He, Z. Zhang, *ACS Omega* **2018**, *3*, 10139.

[22] J. Cui, D. Daniel, A. Grinthal, K. Lin, J. Aizenberg, *Nat. Mater.* **2015**, *14*, 790.

[23] J. Liu, Y. Sun, X. Zhou, X. Li, M. Kappl, W. Steffen, H. J. Butt, *Adv. Mater.* **2021**, *33*, 202100237.

[24] L. Wang, T. J. McCarthy, *Angew. Chem. Int. Ed.* **2016**, *55*, 244.

[25] A. Y. Fadeev, T. J. McCarthy, *Langmuir* **1999**, *15*, 3759.

[26] F. Geyer, M. D'Acunzi, C. Y. Yang, M. Müller, P. Baumli, A. Kaltbeitzel, V. Mailänder, N. Encinas, D. Vollmer, H. J. Butt, *Adv. Mater.* **2019**, *31*, 1801324.

[27] H. Tan, C. Diddens, P. Lv, J. G. M. Kuerten, X. Zhang, D. Lohse, *Proc. Natl. Acad. Sci. USA* **2016**, *113*, 8642.

[28] H. Tan, S. Wooh, H.-J. Butt, X. Zhang, D. Lohse, *Nat. Commun.* **2019**, *10*, 478.

[29] S. A. Vitale, J. L. Katz, *Langmuir* **2003**, *19*, 4105.

[30] M. J. Kreder, D. Daniel, A. Tetreault, Z. Cao, B. Lemaire, J. V. I. Timonen, J. Aizenberg, *Phys. Rev. X* **2018**, *8*, 31053.

[31] Y. Yamauchi, M. Tenjimbayashi, S. Samitsu, M. Naito, *ACS Appl. Mater. Interfaces* **2019**, *11*, 32381.

[32] D. Daniel, J. V. I. Timonen, R. Li, S. J. Velling, J. Aizenberg, *Nat. Phys.* **2017**, *13*, 1020.

[33] C. M. Hansen, *Hansen Solubility Parameters*, CRC Press, **2007**.

[34] K. Manabe, T. Matsubayashi, M. Tenjimbayashi, T. Moriya, Y. Tsuge, K. H. Kyung, S. Shiratori, *ACS Nano* **2016**, *10*, 9387.

[35] R. Krechetnikov, G. M. Homsy, *Phys. Fluids* **2005**, *17*, 102108.

[36] M. J. Hokkanen, M. Backholm, M. Vuckovac, Q. Zhou, R. H. A. Ras, *Adv. Mater.* **2021**, *33*, 2105130.

[37] M. Tenjimbayashi, S. Samitsu, M. Naito, *Adv. Funct. Mater.* **2019**, *29*, 1900688.

[38] L. Limozin, K. Sengupta, *ChemPhysChem* **2009**, *10*, 2752.

Single-solution formed dual-layer liquid-repellent coating: A lubricant layer and lubricant stabilizing base layer are formed from a single solution by the interplay between a solvent evaporation triggered surface lubrication and the interfacial clogging of nanoparticles. This coating is versatile and can be formed on various substrates on a large scale; it exhibits high transparency, self-repairing, and robust omniphobicity to immiscible liquids.

M.T. Author 1 Corresponding Author*
G. H. Author 2, T. H. Author 3, T. U. Author 4

Single-step wet-process formation of dual-layer superslippery coating with transparency and robust omniphobicity

ToC figure (55 mm broad × 50 mm high)